Available online at www.sciencedirect.com
SCIENCE DIRECT
Applied Surface Science 252 (2006) 6294–6303
applied surface science
www.elsevier.com/locate/apsusc

Formation processes of CuCl and regenerated Cu crystals on bronze surfaces in neutral and acidic media

Julin Wang *, Chunchun Xu, Guocheng Lv

Institute of Materials Science and Engineering, Beijing University of Chemical Technology, Beijing 100029, PR China

Received 12 July 2005; received in revised form 21 August 2005; accepted 21 August 2005
Available online 26 September 2005

Abstract

The paper is devoted to investigating the formation of CuCl and regenerated Cu crystals on bronze. Electrochemical behaviour of bronze in simulated anoxic edaphic media and occluded cell (O.C.) solutions was studied with cycle voltammetry (CV) and X-ray diffraction (XRD). Within potential range of −800 to +800 mV, oxidation occurred was largely a process in which Cu is oxidized to CuCl and the reduction process was a reverse of it. An atomic force microscopy (AFM) was used to observe the morphology of CuCl crystals, regenerated Cu crystals and corrosion interface at nm level. The deposition of regenerated Cu on simulated archaeological bronzes was simulated under experimental conditions for the first time. CuCl could be thoroughly reduced to pure Cu if reduction time interval were sufficiently prolonged. This provided a theoretical and experimental basis for getting rid of harmful CuCl patina from archaeological bronzes with electrochemical means.

Keywords: Bronze; Harmful patina; Regenerated Cu; Powdery patina; AFM; Localized corrosion

1. Introduction

It has been long known that the wide existence of powdery patina $Cu_2Cl(OH)_3$ on archaeological bronzes is one of attractive topics in this field [1–6]. Although the process in which harmful patina CuCl is oxidized to $Cu_2Cl(OH)_3$ has been studied for years, one thing deserves to mention here, until now common conclusions on it are not as much as we expected yet [7–12]. In many previous tests archaeological samples were often used to study the further evolvement of CuCl. However, the formation of CuCl was more or less neglected. Having examined corrosion product existed on archaeological bronzes that were excavated at Rome, it came to the conclusion that there are at least two types of patina on ancient bronzes. The first type is chemically stable and does not necessarily require strictly regulated humidity conditions. The second type of patina is related to the presence of chlorides, usually with an accumulation of cuprous chloride. The cuprous chloride formed close to substrate in this case is metastable. Once bronzes with harmful CuCl patina on them are exposed

* Corresponding author. Tel.: +86 10 64445873; fax: +86 10 64214487.
E-mail address: julinwang@126.com (J. Wang).

0169-4332/$ – see front matter
doi:10.1016/j.apsusc.2005.08.041

to atmospheric environment, cuprous chloride will be oxidized to paratacamite or atacamite accompanied with the damage of original corrosion layer [13,14].

The deposition of Cu on archaeological bronze surface is another important issue. As long ago as 1826, Davy carried out an examination on a bronze helmet found in the sea near Corfu. The redeposited crystals of copper was identified on the helmet [13]. Moreover, 11 pieces of archaeological bronzes that were excavated at TaiYuan JinGuo Zhaoqin tomb were examined with metallographic microscopy and SEM-EDX. The free Cu crystals existed on them was concluded as a result of long-term electrochemical corrosion [15]. Some other scholars identified pure Cu crystals that were found on archaeological bronze weapons cast in Wu-Guo. They thought that the deposition of Cu is a mineralization process instead of being simply considered as an electrolysis process. The mineralization process cost so long time that it is impossible to be simulated under experiment conditions [16].

As we know, when metallic artifacts are exposed to soil, sea or atmosphere, most of damage borne by bronzes is largely caused by localized corrosion. Pits and crevices due to localized corrosion are under occluded conditions [17–19]. Localized corrosion occurs in original medium and progresses in occluded solutions. As time elapsed, the pH value and chemical composition of occluded solutions are always quite different from that of original ones. Hence, carrying out tests in both simulated edaphic media and simulated occluded solutions is an essential approach to investigation on the occurring and progressing of bronze corrosion. Since corrosion originally occurs at level of atomic or nm, AFM was used to observe the initial morphology of corrosion product on bronze surfaces [20,21]. The major purpose of the test is to simulate the occurring and progressing of harmful patina CuCl and get rid of them from bronzes. The micro-morphology of corrosion product was observed with AFM and metallographic microscopy.

2. Experimental

2.1. CV spectra

To investigate the electrochemical behaviour of bronze, CV technique was used to obtain in situ electrochemical spectra. The media used in tests were prepared as follows:

Table 1
Chemical compositions and pH values of simulated O.C. solutions (I = 1 mA/cm^2)

Time (h)	SO_4^{2-} (mol/l)	Cl^- (mol/l)	Cu (mmol/l)	Sn (mmol/l)	pH
1	0.0130	0.0267	2.2205	0.0232	6.40
8	0.0224	0.0462	23.3070	0.0329	5.22
16	0.0240	0.0646	36.3779	0.0514	4.92
32	0.0574	0.1486	101.1022	0.0489	4.69

(1) Simulated neutral edaphic aqueous solution containing 0.028 M NaCl, 0.01 M Na_2SO_4 and 0.016 M $NaHCO_3$ (refer to ASTM D1384) [8].
(2) The chemical compositions and the pH values of simulated O.C. solutions are listed in Table 1 [20]. The solutions were achieved by applying positive current 1 mA/cm^2 (to simulate coupling current in and out of O.C.) on bronze specimens for 1, 8, 16 and 32 h, respectively. With the prolonging of electrolysis time period, the pH value dropped and the concentrations of Cl^- and SO_4^{2-} increased. Explanations on these phenomena were dealt with in detail in another paper of the authors' [22]. As a matter of fact, simulated neutral edaphic medium is equivalent to the O.C. solution in which no electrolysis or 0 h electrolysis occurred on bronze specimen.

A Corrtest instrument and a M398 corrosion measurement system manufactured by EG&G [22,23] were used to achieve CV spectra in our tests. Data from them were collected and processed with a computer. The measuring apparatus was a three-electrode system. To simulate the composition of archaeological bronzes, specimens used for working electrode were single α-phase solid solution Cu–Sn alloy, the chemical composition of which was (in wt.%) Cu 94.71, Sn 5.12, Pb 0.17. The exposed area of each specimen was 10 mm × 10 mm along with the remaining were coated with epoxy resin. Each specimen was polished with 300–1200 mesh emery paper, starting with the coarsest grade. Reference electrode used was a saturated calomel electrode (SCE) and auxiliary electrode was a

platinum foil. In order to simulate anoxic environment in O.C., the solution was de-aerated with N_2 for 15 min prior to CV tests. Then the working electrode was polarized at −1.0 V (SCE) for 3 min to remove any oxide film. At ambient temperature, specimen was scanned from −800 to +800 mV, and then reversely scanned to −800 mV at the same rate of 2 mV/s.

2.2. XRD investigations

In order to know the composition of oxidation/reduction product formed in CV, at each peak potential shown in CV spectra, bronze specimens were potentiostatically polarized in anoxic simulated edaphic electrolyte and simulated O.C. solutions, respectively for 1 h. Three oxidation peak potentials were at −10, +400 and +750 mV (in 0 or 1 h simulated O.C. solution). One reduction peak potential was at −400 mV (in 0, 1 or 8 h simulated O.C. solution). A Corrtest system and an American Princeton flat cell with free-electrode system were used in our tests. The area of each working electrode was 17 mm × 17 mm. After required polarization, the specimen was taken out of the cell, rinsed with distilled water and dried. The corrosion product was scraped to a slide, preserved in a desiccator filled with N_2. Analysis was carried out within 2 h. The XRD patterns of corrosion film were recorded with a XRD instrument (DMAX model). With Cu Kα as its radiation source, the instrument worked at sweeping rate of 10°/min, between 10° and 100°, and was operated at 50 kV and 200 mA.

2.3. Metallographic microscopy tests

To observe the metallographic morphology of CuCl and regenerated Cu crystals, bronze specimens were CV scanned to −10, +400, +750 and −400 mV, respectively in anoxic simulated O.C. solution (8 h electrolysis). After scanning, specimens were watered and dried. A $4X_1$ color CCD metallography microscopy and a DMRXA2 micro-polariscope were used to observe the metallographic structures of them immediately. To carry out comparative study with blank specimen, an un-scanned bronze was immersed in nitric acid/alcohol/water (1:1:1) solution for 3 min.

2.4. AFM observations

In order to observe the microstructure of corrosion production, bronze specimens were polished to mirror finish. AFM examinations were carried out on following specimens which were: (i) immersed in simulated neutral edaphic electrolyte for 10 min or, (ii) CV scanned to −10, +750 and −400 mV in simulated neutral edaphic electrolyte, or (iii) CV scanned to −10, +750 and −400 mV, respectively in simulated O.C. solution (8 h electrolysis). A Nanoscope III Digital Instrument system was used at ambient atmosphere. With Si_3N_4 as its needlepoint, the instrument was set at constant-force contacting mode. The unevenness of corroded surface can be distinguished with different grey degree in the same AFM image. Brighter colour represents relative higher area while darker colour represents lower part.

3. Results and discussion

3.1. Formation and progressing of harmful patina CuCl

3.1.1. Electrochemical behaviour of harmful CuCl patina during its formation process

Fig. 1(a) shows the CV spectra of specimens, which experienced 0 and 1 h electrolysis in simulated occluded solutions. In each curve, there is no obvious anodic peak besides one cathodic peak. Current densities increased rapidly with the increase of applied potentials and the maximum of them could be 0.012 A/cm^2 (in 0 h O.C. solution) and 0.016 A/cm^2 (in 1 h O.C. solution), respectively. This revealed that specimen dissolved rapidly [2,5,10]. Dense grey-white spots appeared on the specimen's surface. Corrosion pits were clearly visible on specimen after the spots were polished away. This demonstrated the occurrence of pitting corrosion in oxidation process. To identify the composition of corrosion product that formed in oxidation process, bronze specimens were anodically polarized for 1 h at −10 mV (initial potential), +400 mV (intermediate potential) and +750 mV (almost the highest potential) respectively in simulated O.C. solutions (0 and 1 h electrolysis). Examined with XRD, besides bronze substrate, CuCl is illustrated in Fig. 2.

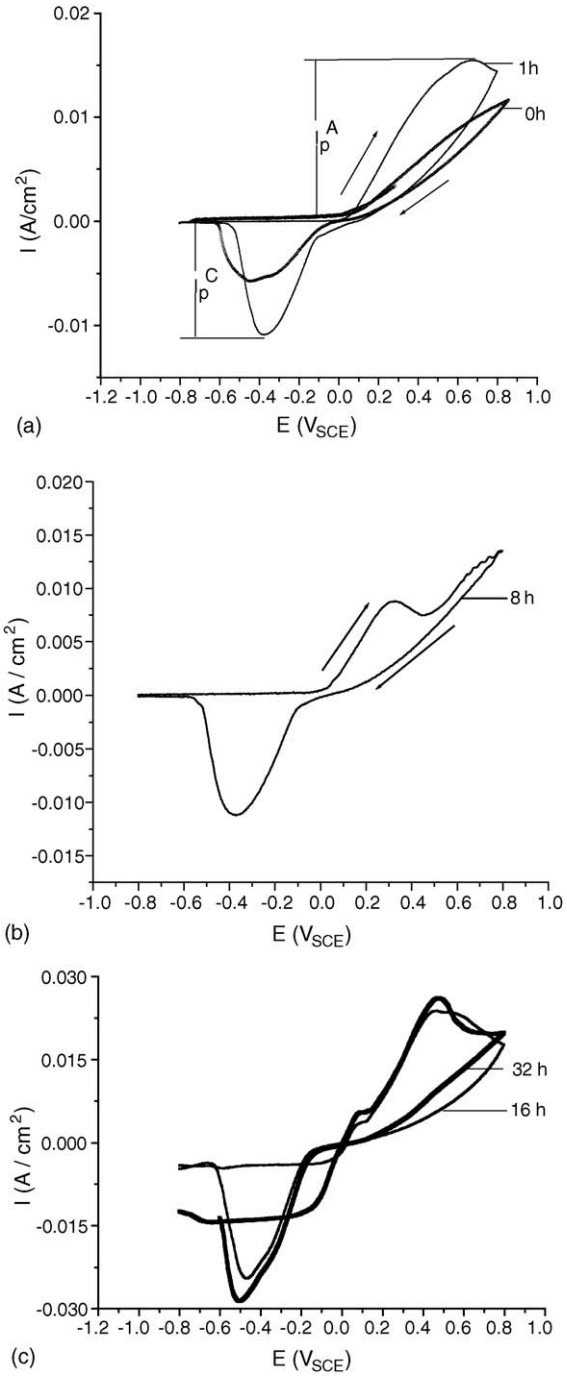

Fig. 1. CV spectra of bronze in simulated O.C. solutions of different electrolysis intervals (scan rate: 2 mV/s).

Fig. 1(b) shows CV spectrum achieved with specimen in simulate O.C. solution (8 h electrolysis). Comparing with Fig. 1(a), anodic peak appeared at +300 mV and was followed with a short current density platform. Then current density increased linearly with the increase of applied potential. This indicated that the corrosion product formed at +300 mV could hardly provide any protection for the substrate. Bronze specimens were anodically polarized for 1 h at −10 mV (initial potential), +300 mV (peak potential) and +750 mV (near to the highest potential), respectively in simulated O.C. solutions (8 h electrolysis). Shown in Fig. 2, the grey-white corrosion product was proved to be CuCl with XRD examination.

Fig. 1(c) shows the CV spectra achieved with bronze specimens in simulated O.C. solutions (16 and 32 h electrolysis). Comparing with Fig. 1(a) and (b), one faint and one strong, two anodic peaks appeared in each curve shown in Fig. 1(c). Most of the corrosion product formed at each oxidation peak (+80 or +470 mV) was identified to be CuCl with XRD examination. In Fig. 1(a) and (b), current densities were quite low (nearly zero) during positive scanning from −800 to −10 mV. Furthermore, in Fig. 1(c), current density appeared negative within the same scope of scanning potential. This is because the concentration of copper ions in solutions (16 and 32 h electrolysis) became so high that copper ions started to be reduced to Cu.

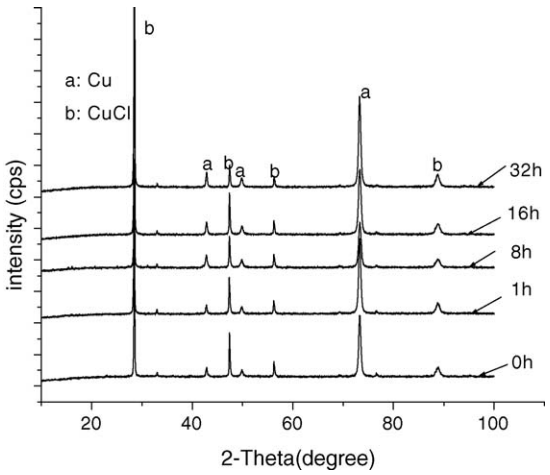

Fig. 2. XRD patterns of bronze oxidation process in simulated O.C. solutions.

Comparison with Fig. 1(a–c) shows that the longer electrolysis time interval in O.C, the higher current densities were in oxidation/reduction processes, and the faster corrosion rates were. This phenomenon was led by two factors. Firstly, the concentration of copper ions became higher along with the prolonging of electrolysis time period in O.C.; secondly, the solution became more corrosive because of acidification effect. During positive scanning from −800 to −10 mV, current densities were nearly zero (i.e. almost no oxidation/reduction occurred on specimens) or negative (i.e. copper ions were reduced). Anodic reaction (formation of CuCl) started when scanning potential was above −10 mV. Current densities started to increase rapidly along with positive scanning.

3.1.2. Progressing of harmful CuCl patina

In CV test, the formation of harmful CuCl patina was successfully simulated in anoxic edaphic electrolyte. In order to research how CuCl on bronze artifact was affected by atmospheric oxygen and moisture after excavation, two bronze specimens were anodically polarized at +400 mV for 1 h in simulated neutral edaphic electrolytes to artificially form harmful patina CuCl on them. Then specimens were exposed to ambient atmosphere for 3 or 15 days, respectively and wetted with distilled water every 8 h. Shown in Fig. 3, CuCl was thoroughly oxidized to powdery patina $Cu_2Cl(OH)_3$. Due to difference in molar volumes (CuCl 3.36 versus $Cu_2Cl(OH)_3$ 3.99), corrosion layer became thicker and looser. Additionally, crack progressed on the surface. Powdery patina broke out to surface from inner substrate. This is consistent with the conclusion drawn by Fan that CuCl, rather than Cu_2O, was initially formed and then oxidized to powdery patina $Cu_2Cl(OH)_3$ [24].

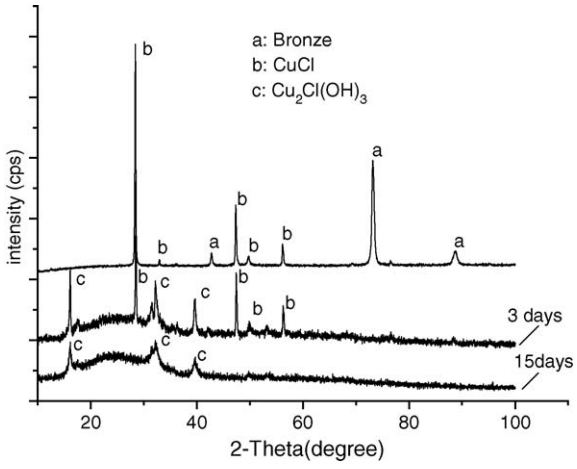

Fig. 3. The evolution of CuCl.

Described as above, CuCl did harm to bronzes as following:

(1) In anoxic water solution, CuCl reacted with H_2O as following:

$$2CuCl + H_2O = Cu_2O + 2HCl \quad (1)$$

After being formed in the reaction, HCl accelerated the dissolution of bronze and then more CuCl were formed. This is referred to as the self-catalysis effect of CuCl.

(2) In aerobic and moist environment, CuCl reacted with O_2 and H_2O as following:

$$4CuCl + O_2 + 4H_2O = 2Cu_2Cl(OH)_3 + 2HCl \quad (2)$$

Powdery patina $Cu_2Cl(OH)_3$ were formed together with HCl.

3.1.3. Micro-morphology of CuCl

Bronze and its behavior are best elucidated by metallography. Generally, bronze corrosion is closely tied to its metal structure and composition. Single-phase bronzes are often encountered in the Far East (particularly in early China) as well as in the West. Studies of corrosion mechanisms in the West have so far concentrated on single- or mono-phase bronzes [25]. Because many archaeological bronzes had experienced post-treatment after cast [26,27], single α-phase solid solution Cu–Sn alloy that had experienced hot-forging and annealing treatments was selected as specimens to simulate the metallographic structure of archaeological bronze in the test. Re-crystals grain and twin-crystals are illustrated in Fig. 4(a). Cavity and lattice defects existed on crystals provided initial place for corrosion occurred at ambient temperature. Fig. 4(b) and (c) are metallographic images that CuCl were formed on bronze surface after specimens were anodically polarised at −10 or +750 mV, respectively in simulated O.C. solution (8 h electrolysis).

In Fig. 1(b), when scanning potential was above −10 mV, polarization current density began to

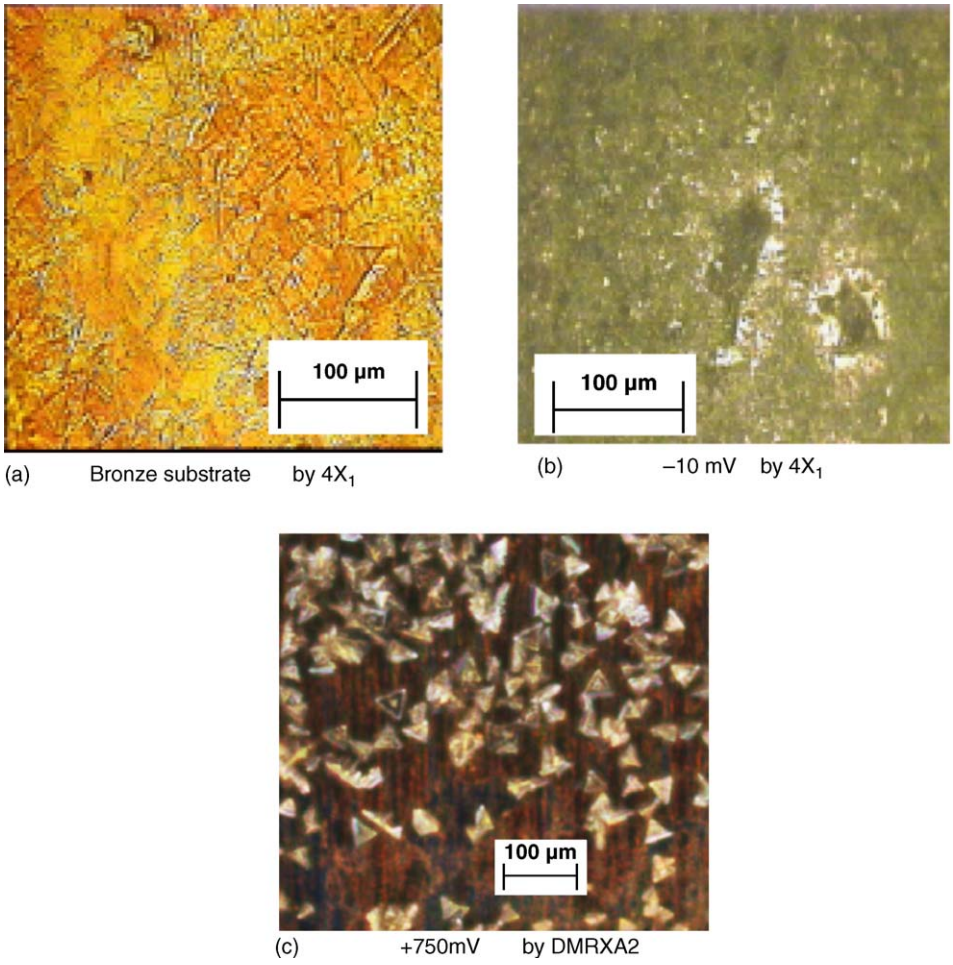

Fig. 4. The metallographic pictures of bronze in simulated O.C. solution (8 h electrolysis) at anodic potentials.

increase rapidly. Shown in Fig. 4(b), a few CuCl was formed on electrode surface with pits at partial area. This revealed the occurrence of localized corrosion. Fig. 4(c) shows that the fine crystals formed at −10 mV had obviously grown larger in triangular shape when specimen was CV scanned to +750 mV. Triangular shape revealed the typical characteristic of CuCl {1 1 1} crystals groups. In addition to say, CuCl layer formed in test was not compact.

After AFM examination, the morphology of CuCl that was at its initial formation stage is illustrated in Fig. 5. Shown in Fig. 1(a), bronze specimen was positively scanned to −10 mV in O.C. solution (0 h electrolysis). The morphology of CuCl formed at this potential can be seen in Fig. 5(a). The surface is corroded intensively and pits appeared (about 105 nm deep). Within scan size of 2 μm × 2 μm, most of CuCl appeared as tiny crystals at nm level. Some of them grew around crystals cores and became larger ones. Shown in Fig. 5(b), when scanning potential was above +750 mV, CuCl crystals grew rapidly up to approx. 5 μm wide and 9 μm high in average. Within scan size of 10 μm × 10 μm, the disordered arrangement of CuCl crystals on substrate could be observed.

With comparison between Fig. 5(a) and (b), the sizes of CuCl crystals were proved to increase with the increasing of applied potentials in oxidation process. Bronze specimen suffered localized corrosion in this process. According to the height of crystals along *Z*-axis

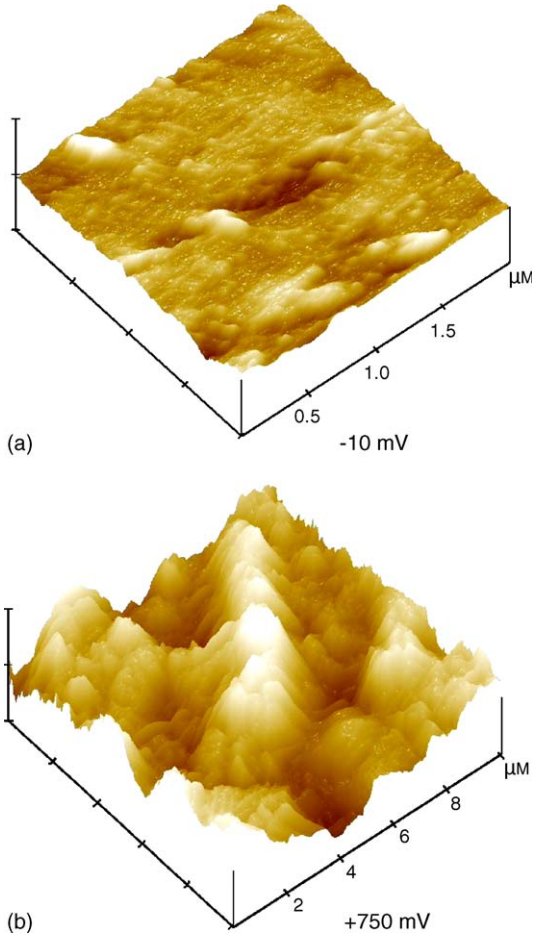

Fig. 5. AFM images of bronze in simulated neutral edaphic electrolyte at different potentials.

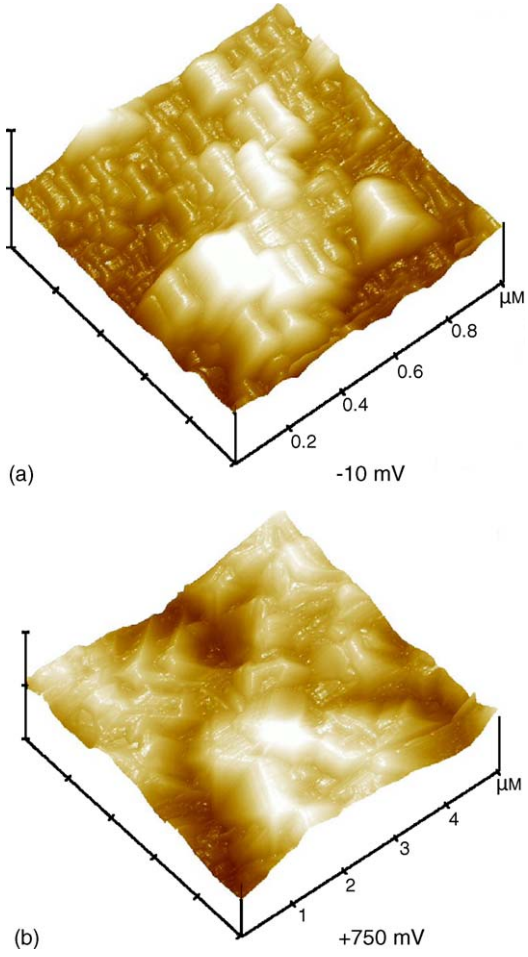

Fig. 6. AFM images of CuCl on bronze at anodic potentials.

in each AFM image, the roughness and unevenness of corroded bronze surface changed markedly.

To observe the growth morphology of CuCl during the evolvement of localized corrosion, bronze was examined with AFM at different scanning potentials in O.C. solution (8 h electrolysis). When specimen was CV scanned to −10 mV, a three-dimensional image of CuCl formed at this potential within scan area of 1 μm × 1 μm is shown in Fig. 6(a). At their initial growing period, CuCl crystals arrange regularly on most area of the substrate. The minimum width of crystals is about 51 nm and the maximum is about 154 nm. In Fig. 6(b) specimen was CV scanned to +750 mV and observed within the size of 5 μm × 5 μm. Comparing with Fig. 6(a), the size of CuCl crystals in Fig. 6(b) was much larger. The free growing directions of crystals were prohibited and had to turn to other directions. Crystals arranged irregularly and the surface obviously looked more rough and uneven.

3.2. Growth of regenerated Cu crystals

3.2.1. Electrochemical behaviour and XRD examination during the growth of regenerated Cu crystals

There is one reduction peak in each CV curve shown in Fig. 1(a–c). To identify the composition of reduction product formed at each reduction peak in simulated O.C. solutions (0 and 8 h), bronzes were

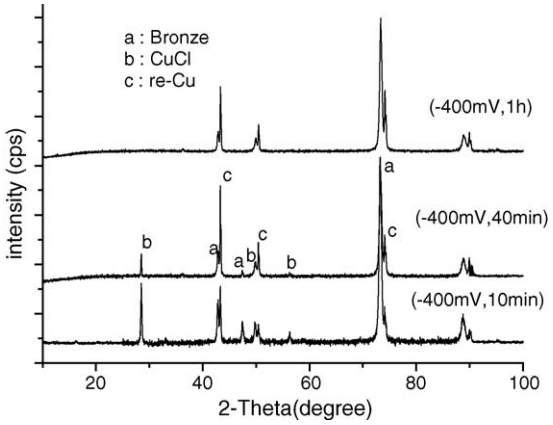

Fig. 7. XRD patterns of reduction production and the effect of reduction time (in simulated 8 h electrolysis O.C.solution).

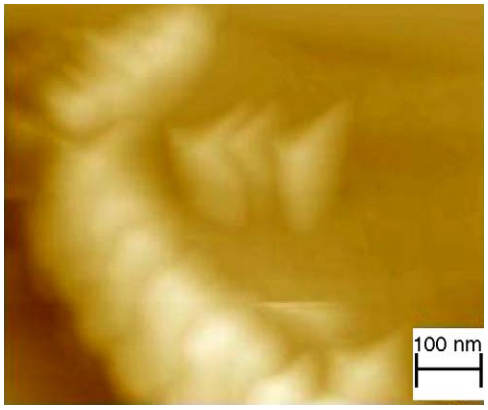

Fig. 8. the AFM image of pure Cu separated out when bronze was in simulated O.C. solution (8 h electrolysis).

anodically polarized at +300 mV for 10 min, then anodically polarized at +750 mV for another 10 min, and finally cathodically polarized at −400 mV for the last 10 min. XRD examination on these specimen revealed that the black colour production was regenerated Cu (besides bronze substrate). Shown in Fig. 7, although not all of CuCl was reduced to pure Cu in occluded solution (8 h electrolysis), however, this was realized when reduction time period was prolonged to 1 h.

In Fig. 1(a–c), reduction occurred in potential range of +15 to −600 mV. If specimen were polarized within this potential range for sufficient time period, all of CuCl could be reduced to Cu. This provided a theoretical and experimental basis for getting rid of harmful CuCl patina from bronze artifacts with electrochemical manner. In fact, potential is from −50 to +250 mV (SCE) and the pH value is from 4.5 to 9.0 in practical soil [9]. Under such conditions, one hand, bare state specimen will lead to the taking place of oxidation; on the other hand, specimen covered with corrosion product such as CuCl will lead to the occurrence of reduction. Generally, part of substrate is bare while the remaining is covered with corrosion product. Therefore, oxidation and reduction can occur simultaneously on one specimen. This explains how corrosion product and regenerated Cu crystals can coexist on the same excavated bronze [15]. The deposition of regenerated Cu crystals was successfully simulated at experimental conditions and this will be helpful for further research on bronze corrosion mechanism. Not as some scholars thought that the formation of pure Cu crystals needs to take so long time that it can not be simulated in experiment at all [16], as a matter of fact, the existence of regenerated Cu crystals on bronze can no longer be considered as a base to judge whether it is a real archaeological bronze or a fake [28].

3.2.2. *Micro-morphology of regenerated Cu crystals*

The AFM image of regenerated Cu crystals that deposited at −400 mV in simulated O.C. solution (8 h electrolysis) is shown in Fig. 8. Some of nm level Cu crystals deposited on bronze substrate in similar shape but different sizes. The minimum crystals was about 80.06 nm high and 203.13 nm wide.

Fig. 9 shows metallographic image of Cu crystals that deposited at −400 mV in simulated occluded solution (8 h electrolysis). Some of CuCl was reduced to Cu. The growth and distribution of free Cu crystals can be observed with different examination instruments. In Fig. 9(a), being prohibited in free growing directions, regenerated Cu crystals had to grow toward other directions. In Fig. 9(b), regenerated Cu distributed tightly or in bits and pieces on the substrate. Some of them could be found in corroded grooves. Holes and cracks are clearly visible in these images.

Mentioned as above, after examinations with XRD, AFM and metallographic microscope, it was proved possible to reduce harmful CuCl patina to harmless Cu crystals with electrochemical manner. In addition to it, complex chloride ions were changed into free chloride

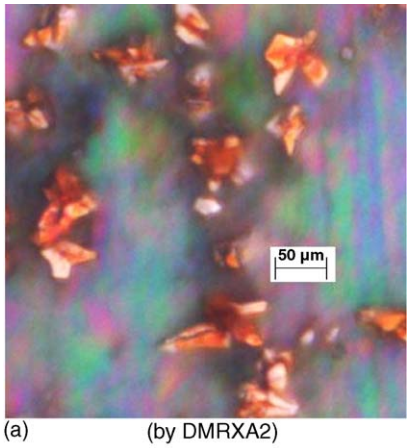

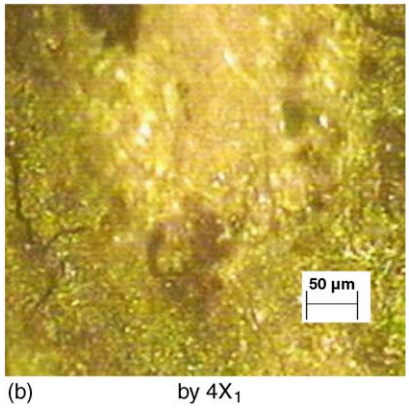

Fig. 9. the metallographic pictures of regenerated Cu when bronze was in simulated O.C. solution (8 h electrolysis).

ions that are easier to eliminate as an important corrosive factor.

3.3. Variety of crystals structure of corrosion product

Fig. 10 shows the comparison among XRD patterns of (i) CuCl formed in simulated neutral edaphic electrolyte, (ii) regenerated Cu and (iii) bare substrate. Described as above, the bronze specimens used were made of single α-phase solid solution. Formed with dissolving Sn into Cu, α-phase is a kind of uniform solid solution which has the same crystals lattice (face-centered cubic structure) as pure Cu crystals has. The diffraction peaks of α-phase appeared close to that of regenerated Cu. The differences in interplanar distances (*d* values) between α-phase and regenerated

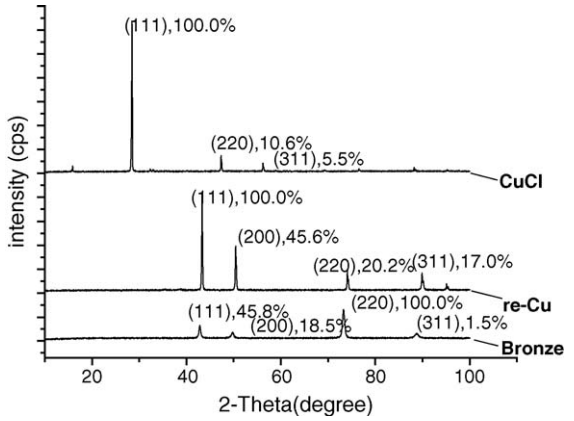

Fig. 10. the change of structures of crystal during corrosion process.

Cu are quite few. *d* values of the former are merely a little higher than those of the latter. This is because the radius of Sn atom is a little bigger than that of Cu. Hence the lattice parameter of α-phase is increased. Fig. 10 shows that the crystals structures of bronze substrate, regenerated Cu and CuCl all belong in poly-crystals. The differences among these crystals are as follows: (i) {2 2 0} crystals face groups take absolute majority in α-phase bronze, (ii) {1 1 1} crystals face groups dominate in CuCl, and (iii) {1 1 1} crystals face groups take absolute majority in regenerated Cu. Both CuCl and regenerated Cu belong in the same {1 1 1} crystals face group, however, the crystals face distance of the former is much higher than that of the latter (3.12 versus 1.85). Therefore, the crystals structure varied apparently during oxidation/reduction process.

4. Conclusions

(1) With bronze specimens (Cu 94.71, Sn 5.12, Pb 0.17 in wt.%) in anoxic simulated neutral edaphic media and simulated O.C. solutions, within the potential range of −800 to +800 mV, the oxidation of bronze was mainly a formation process of CuCl. Extending localized corrosion time period, polarization current increased and the bronze substrate was intensively damaged. Reduction occurred was a process by which CuCl was reduced to regenerated Cu. The formation of regenerated Cu can be simulated at experimental conditions and these conditions also exist in practical soil.

(2) Harmful CuCl patina could continue to be oxidized to powdery patina $Cu_2Cl(OH)_3$ when bronze with CuCl was exposed to moist atmosphere.
(3) With sufficient time period of reduction, CuCl was completely reduced to regenerated Cu. This proved the feasibility of getting rid of harmful CuCl patina from archaeological bronzes with electrochemistry manner and provided a theoretical and experimental base for it.

Acknowledgements

The authors would like to express their gratitude for the financial support from National Key Technologies R&D Programme of the 10th Five-year Plan Period and the State Key Laboratory of Metallic Corrosion and Protection. They are also grateful to Ms. Zhao Xiufeng and Dr. Fang Yikun for their assistance on testing work.

References

[1] B. Millet, C. Fiaud, C. Hinnen, A correlation between electrochemical behaviour, composition and semi-conducting properties of naturally grown oxide films on copper, Corros. Sci. 37 (12) (1995) 1903–1918.
[2] G. Laguzzi, L. Tommesani, L. Luvidi, Thin layer activation technique application in bronze corrosion monitoring, Corros. Sci. 41 (1999) 197–202.
[3] Giuseppe Laguzzi, Loredana Luvidi, Giancarlo Brunoro, Atmospheric corrosion of B6 bronze evaluated by the thin layer activation technique, Corros. Sci. 43 (2001) 747–753.
[4] E. Geler, D.S. Azambuja, Corrosion inhibition of copper in chloride solutions by pyrazole, Corros. Sci. 42 (2000) 631–643.
[5] J. Davy, Observations on the changes which have taken place in some ancient alloys of copper, Phil. Trans. R. Soc. Lond. 116 (3) (1826) 55–59.
[6] Gao Yin, China History Museum Publication, 1 (1979) 121–124.
[7] I. Constantinides, A. Adriaens, F. Adams, Surface characterization of artificial corrosion layers on copper alloy reference materials, Appl. Surf. Sci. 189 (2002) 90–101.
[8] L. Robbiola, J. Blengino, C. Fiaud, Morphology and mechanism of formation of natural patinas of archaeological Cu–Sn alloys, Corr. Sci. 40 (12) (1998) 2083–2111.
[9] I. Mabille, A. Bertrand, E.M. Surtter, Mechanism of dissolution of a Cu–13Sn alloy in low aggressive conditions, Corros. Sci. 45 (2003) 855–866.
[10] R.M. Organ, Stud. Conserv. 8 (1963) 1–6.
[11] Fan. Chongzheng, Wang. Changsui, Wang. Shengjun, Sci. China (Series B) 3 (1991) 239–245.
[12] Guan Yulong, Du Min, Bronze disease: a review of some chemical problems and the role of relative humidity, Sci. Conserv. Archaeol. 5 (1) (1993) 56–63 (Translation).
[13] David A. Scott, Bronze disease: a review of some chemical problems and the role of relative humidity, J. Am. Inst. Conserv. 29 (2) (1990) 193–206.
[14] David A. Scott, An examination of the patina and corrosion morphology of some Rome bronzes, J. Am. Inst. Conserv. 33 (1) (1994) 1–23.
[15] Sun. Shuyun, Analysis of bronze artifacts excavated from TaiYuan JinGuo ZhaoQing Tomb, Papers China Metall. Hist. (3 A) 4 (2002) 178–185.
[16] Jia Yin, Su Rongyu, Hua Jueming, The Primary study of regenerated Cu crystals formation mechanism in corroded bronze artifacts, Sci. Conserv. Archaeol., 11 (2) (2000) 154–163.
[17] Zuo. JingYi, M. Pourbaix, Xu ChunChun, Kinetic and thermodynamic behaviour inside occluded corrosion cells interpreted by potential/pH Diagrams*, Corros. Sci. 29 (5) (1989) 557–566.
[18] Zuo. JingYi, M. Pourbaix, Xu. ChunChun, Potential–pH diagrams of stress effects on occluded cell corrosion inside stress corrosion cracks, Corrosion 51 (30) (1995) 177–184.
[19] Zu. Hongfan, Zhou. Hao, Relationship between bronze disease occurrence and hole corrosion, Electrochemistry 5 (3) (1999) 7–12.
[20] R.A. Silva, M. Walls, B. Rondot, Electrochemical and microstructural studies of tantalum and its oxide films for biomedical applications in endovascular surgery, J. Mater. Sci.: Mater. Med. 13 (2002) 495–500.
[21] V.B. Singh, A. Gupta, The electrochemical corrosion and passivation behaviour of Monel (400) in concentrated acids and their mixtures, J. Mater. Sci. 36 (2001) 1433–1442.
[22] Xu ChunChun, Wang JuLin, Investigation of the chemical and electrochemical behaviour of mass transfer at an archaeological bronze/soil interface, Anti-corros. Meth. Mater. 50 (5) (2003) 326–333.
[23] Xia. Cao, Chunchun. Xu, Weizhen. Ouyang, A comparative study on the corrosion behaviour of simulated archaeological iron in Cl^-, NO_3^- and HSO_3^- bearing pollutants, Anti-corros. Meth. Mater. 52 (4) (2005) 207–213.
[24] Fan. Chongzheng, Hu. Keliang, Wu. Youshi, Sci. Conserv. Archaeol. 9 (1) (1997) 20–24.
[25] Thomas. Chase, Investigation of ancient bronzes S International congress on the conservation and restoration for archaeological objects February 14–16, 2002, 9–28.
[26] Sun. Shuyun, Identificatin and investigation of bronze artifacts from DongHuishan Site SiBa culture, Papers China Metall. Hist. (3 A) 4 (2002) 203–208.
[27] Li. XiuHui, Han. Rubeng, The metallography study of bronze ware excavated from Zhukaigou Site, Papers China Metall. Hist. (3 A) 4 (2002) 242–260.
[28] Yao. QingFang, The investigation on the composition of Simuwu Tripod and the application of artifacts protection technology on archaeological bronzes study, in: Proceedings of the Seventh National conference on archaeology and artifacts protection, vol. 10, 2002, pp. 98–100.